Respiratory Research

RESEARCH

Open Access

Aging shapes infection profiles of influenza A virus and SARS-CoV-2 in human precision-cut lung slices

Melanie Brügger[1,2*], Carlos Machahua[3,4], Trix Zumkehr[1,2,10], Christiana Cismaru[1,2,5,11], Damian Jandrasits[1,2,5,12], Bettina Trüeb[1,2], Sara Ezzat[1,2,5], Blandina I. Oliveira Esteves[1,2], Patrick Dorn[6], Thomas M. Marti[6,7], Gert Zimmer[1,2], Volker Thiel[1,2,8,9], Manuela Funke-Chambour[3,4] and Marco P. Alves[1,2,8*]

Abstract

Background The coronavirus disease 2019 (COVID-19) outbreak revealed the susceptibility of elderly patients to respiratory virus infections, showing cell senescence or subclinical persistent inflammatory profiles and favoring the development of severe pneumonia.

Methods In our study, we evaluated the potential influence of lung aging on the efficiency of replication of influenza A virus (IAV) and severe acute respiratory syndrome coronavirus 2 (SARS-CoV-2), as well as determining the pro-inflammatory and antiviral responses of the distal lung tissue.

Results Using precision-cut lung slices (PCLS) from donors of different ages, we found that pandemic H1N1 and avian H5N1 IAV replicated in the lung parenchyma with high efficacy. In contrast to these IAV strains, SARS-CoV-2 Early isolate and Delta variant of concern (VOC) replicated less efficiently in PCLS. Interestingly, both viruses showed reduced replication in PCLS from older compared to younger donors, suggesting that aged lung tissue represents a suboptimal environment for viral replication. Regardless of the age-dependent viral loads, PCLS responded to H5N1 IAV infection by an induction of IL-6 and IP10/CXCL10, both at the mRNA and protein levels, and to H1N1 IAV infection by induction of IP10/CXCL10 mRNA. Finally, while SARS-CoV-2 and H1N1 IAV infection were not causing detectable cell death, H5N1 IAV infection led to more cytotoxicity and induced significant early interferon responses.

Conclusions In summary, our findings suggest that aged lung tissue might not favor viral dissemination, pointing to a determinant role of dysregulated immune mechanisms in the development of severe disease.

Keywords Influenza virus, SARS-CoV-2, Aging, Precision-cut lung slices, Distal lung

*Correspondence:
Melanie Brügger
melanie.bruegger@unibe.ch
Marco P. Alves
marco.alves@unibe.ch
Full list of author information is available at the end of the article

Introduction

Viral pneumonia induced by influenza A virus (IAV) and severe acute respiratory syndrome coronavirus 2 (SARS-CoV-2) is a leading cause of death from infectious diseases worldwide [1–3]. Importantly, there is a profound difference in clinical severity of coronavirus disease 2019 (COVID-19) depending on age. Specifically, while advanced age is associated with higher risk for severe disease and death, children are rarely affected, and severe pneumonia is unusual in this population [4]. On the other hand, infection by IAV is associated with increased mortality in older patients, but also poses a risk for severe disease in young children [5–7].

The increased susceptibility of the elderly to severe respiratory virus infections is due to a combination of factors associated with aging, including comorbidities, a decline in lung function, cellular senescence, and dysregulated immunity. This includes impairment of local innate immune mechanisms, an hyperinflammatory phenotype related to age called "inflammaging", and a decline in humoral and cellular responses, termed "immunosenescence" [8–10]. Infection with a number of viruses, such as measles virus, human respiratory syncytial virus, and coronaviruses, can induce premature cellular senescence [11]. Interestingly, infection of lung tissue by IAV induced premature aging as indicated by the appearance of senescent cells and subsequently, infection of senescent cells resulted in increased viral replication [12]. Similarly, SARS-CoV-2 was shown to induce senescence through multiple mechanisms with the potential to trigger COVID-19-related "cytokine storm" and organ damage [13].

Nevertheless, the impact of age and the local pulmonary microenvironment on acute respiratory virus infection has not been elucidated so far, mainly due to experimental limitations and because no suitable animal model is available. Previous studies utilizing lung explants, including unprocessed lung biopsies [14–18] and precision-cut lung slices (PCLS) [19], have demonstrated the high efficiency of IAV replication in cultured lung tissue from the lower respiratory tract, making them valuable models for studying IAV infection and virulence. Lung explants have also been used to study the replication potential of SARS-CoV-2 variants, the cellular tropism of both SARS-CoV and SARS-CoV-2, and the subsequent immune responses [17, 18, 20, 21]. However, these studies did not examine the influence of the tissue donors' age. Of note, we and others have demonstrated an age-dependent susceptibility of the upper respiratory epithelium towards respiratory virus infection [22, 23]. Thus, we hypothesized that the features of the lung from older individuals, particularly the alveolar epithelium of the distal lung, may influence viral replication and contribute to the adverse outcomes during IAV or SARS-CoV-2 infections in the elderly. We employed a model of respiratory virus infection based on PCLS cultures [24–27]. This culture model preserves the bronchiolar and alveolar structures with minimal changes during culture for up to two weeks [28], allowing the study of cell behavior and cell–cell interactions in their native cellular environment [27]. Due to these characteristics, PCLS are bridging the gap between simple in vitro and complex in vivo systems [25], by recapitulating pathophysiological conditions and local inflammatory responses, that are believed to occur in vivo [29]. The generation of defined tissue sections ensures better homogeneity and reproducibility, thus reducing the degree of variability between the replicates [30, 31].

In this study, we investigated IAV and SARS-CoV-2 replication and pro-inflammatory and antiviral responses induced by infection of "older" *versus* "younger" distal lung tissue. We used human PCLS, obtained from several donors with different ages, for viral infection studies using an early isolate of SARS-CoV-2 and an isolate of the Delta VOC, as well as the 2009 pandemic IAV H1N1 and avian IAV H5N1.

Materials and methods

Biosafety statement

All experiments with infectious H5N1/A/turkey/Turkey/1/2005 and SARS-CoV-2 were performed in an enhanced biosafety level 3 (BSL3) containment laboratory at the Institute of Virology and Immunology, Mittelhäusern, Switzerland, which followed the approved standard operating procedures of BSL3 facility of relevant authorities in Switzerland (authorization no. A202819). All the personnel involved in these experiments received advanced training and wore appropriate personal protective equipment, including Tyvek overall and hood, and a Jupiter or Versaflo respirator with an HEPA filter system (all 3 M).

Cell lines and culture conditions

Madin-Darby canine kidney type II (MDCK-II) cells were kindly given by Georg Herrler (University of Veterinary Medicine Hannover, Germany) and were cultured in MEM (Thermo Fisher Scientific) supplemented with 5% fetal bovine serum (FBS). Human embryonic kidney 293 T (HEK-293 T) cells (American Type Culture Collection (ATCC), Manassas, USA; CRL-3216), were maintained in DMEM supplemented with 10% FBS. VeroE6 cells were kindly provided by Doreen Muth, Marcel Müller, and Christian Drosten (Charité, Berlin, Germany) and cultured in DMEM GlutaMax supplemented with 10% FBS and 1% HEPES (all Thermo Fisher Scientific). VeroE6-TMPRSS2 cells (NIBSC Research Reagent

Depository, UK) were cultured in DMEM GlutaMAX with 10% FBS and 1X non-essential amino acids (Thermo Fisher Scientific). When passaging, 200 µg/ml of geneticin (G418) were added to the culture medium. All cells were maintained in a humidified incubator at 37 °C, 5% CO_2.

Human precision-cut lung slice cultures

Human PCLS were prepared as previously reported by us [32, 33]. Briefly, lung tissue distant from the tumor edges resections (tumor-free margin of a minimum of 5 cm), with no signs of inflammation or emphysema, were collected at the Inselspital, Bern University Hospital (approved by the Bernese Ethics Commission, license: KEK-BE_2018-01801). All donors were informed and signed a written consent before inclusion. All lung tissue resections were tested for SARS-CoV-2 by qPCR. Once in the lab, tissues were processed within six hours post-surgery: 1 cm^3 low-melting agarose-perfused (2%) lung tissues were cut in 400 µm slices in the Compresstome VF-310-0Z Vibrating Microtome (Precisionary), following the manufacturer's recommendations. Slices were placed in 12-well plates with DMEM GlutaMax medium, 1% FBS, HEPES 20 mM, and 1X Antibiotic–Antimycotic (Thermo Fisher). PCLS were incubated at 37 °C, 5% CO_2 in a humidified incubator, and medium was changed every day for one to seven days prior infection.

Human well-differentiated primary nasal epithelial cells

Generation of human well-differentiated nasal epithelial cell cultures (WD-NECs) was done as previously described [32]. In short, primary NECs were obtained commercially (Epithelix Sàrl, Geneva, Switzerland). Cells were seeded and maintained on 24-well transwell inserts (Corning) at the air–liquid interface in MucilAir culture medium (Epithelix Sàrl, Geneva, Switzerland) in a humidified incubator at 37 ℃, 5% CO_2. Culture medium was changed every three days.

Viruses

The eight-plasmid pHW2000 reverse genetics system of H1N1 A/Hamburg/4/2009 (GenBank accession nos.: GQ166207, GQ166209, GQ166211, GQ166213, GQ166215, GQ166217, GQ166219, GQ166221) was provided by Hans-Dieter Klenk (University of Marburg, Marburg, Germany). For generation of infectious virus, 10^6 MDCK-II cells and 2×10^6 HEK-293 T cells were seeded into 10 cm cell culture dishes and grown overnight at 37 °C, 5% CO_2. The co-culture was transfected with the 8-plasmid set (2 µg of each plasmid) using Lipofectamine 2000 transfection reagent (Fisher Scientific). At 24 h post transfection, the cells were washed with PBS and maintained in serum-free medium supplemented with 0.2% (w/v) of bovine serum albumin (BSA), 1% (v/v) of penicillin/streptomycin, and 1 µg/ml of acetylated trypsin. Passage 0 was obtained six days post-transfection, when the cell medium was collected, FBS was added to a final concentration of 5% and cell debris was removed by centrifugation (3000 rpm, 10 min, 4 °C). Two passages on MDCK-II, in the presence of trypsin, were performed to obtain the working stock, which was titrated on MDCK-II cells, as described below, before use. H5N1 A/turkey/Turkey/2005 was kindly provided by Dr. W. Dundon, (IZSV Instituto Zooprofilattico Sperimentale delle Venezie, Venice, Italy). Virus was passaged twice in embryonated chicken eggs and allantoic fluid was clarified using low-speed centrifugation as described previously [34]. A SARS-CoV-2 early isolate (SARS-CoV-2/München1.1/2020/929, "Early isolate" in subsequent text and figures), kindly provided by Daniela Niemeyer, Marcel Müller, and Christian Drosten (Charité, Berlin, Germany), was passaged once in VeroE6 cells. To produce the working stock, SARS-CoV-2 Early isolate was then propagated once more in VeroE6 cells at a multiplicity of infection (MOI) of 0.01 plaque forming unit (PFU) per cell. Therefore, the respective volume of the original isolate was added to the cells in DMEM GlutaMax supplemented with 10% FBS and incubated for 36 h at 37 °C, 5% CO_2. SARS-CoV-2 Delta isolate (SARS-CoV-2 Delta AY.127 (hCoV-19/Switzerland/BE-IFIK-918–4879/2021, L5109, passage of EPI_ISL_1760647)) [35] was passaged three to four times accordingly on VeroE6-TMPRSS2 cells. Next, the supernatant was centrifuged to eliminate cell debris, and then stored in aliquots at − 70 °C. Next, we performed whole genome sequencing of the SARS-CoV-2 virus stocks used for the infection experiments, with special focus on the polybasic cleavage site of the spike protein, due to previous observation of rapid cell culture-induced mutations [36]. We performed sequencing on viral RNA isolated from SARS-CoV-2 Early isolate- and Delta-infected VeroE6-TMPRSS2 cells. We generated sequencing libraries using the Rapid Barcoding Kit 96 V14 (SQK-RBK114.96) ONT (Oxford Nanopore Technologies, https://nanoporetech.com) and sequenced on an ONT MinION according to the manufacturer's instructions. We used ONT MinION software version 24.2.16 to perform data acquisition and real-time high-accuracy basecalling. Geneious Prime 2024.0.4 was used to map (minimap2) fastq pass reads to the reference SARS-CoV-2/Wuhan-Hu-1 (GenBank accession no. MN908947.3) to find variations and to create a consensus sequence. We aligned the consensus sequences of the Early and Delta isolates, and the reference Wuhan to assess the polybasic cleavage site of the spike protein (Fig. S1A).

Infection of human precision-cut lung slice cultures

PCLS were infected one to seven days post-surgery and experiments were conducted within four to ten days post-surgery. Similarly-sized PCLS were infected with either Mock or virus at 10^6 PFU of IAV H5N1/A/turkey/Turkey/2005 and H1N1/Hamburg/4/2009 or SARS-CoV-2 Early and Delta isolate, in 750 µL infection medium (DMEM GlutaMAX, supplemented with 0.1% FBS, 100 units/ml of penicillin and 100 µg/ml streptomycin, and 2.5 µg/ml of Amphotericin), for 2 h at 37 °C, 5% CO_2. Afterwards, PCLS were washed twice with PBS with Ca^{2+} and Mg^{2+}, to remove residual virus inoculum and then fresh growth medium (DMEM GlutaMAX, supplemented with 1% FBS, 100 units/ml of penicillin and 100 µg/ml streptomycin, and 2.5 µg/ml of Amphotericin) was added. Every 24 h medium was changed and 4, 24, 48, and 72 h post-infection (h p.i.), PCLS were collected for RNA extraction in ice-cold TRIzol reagent (Thermo Fisher) or washed twice in PBS, transferred to embedding cassettes, and then fixed in 4% formalin for 24 h until further processing for immunohistochemistry and immunofluorescence staining. Supernatants from indicated timepoints were collected before the daily medium change and frozen at − 70 °C until further processing.

RNA isolation and quantitative PCR

RNA isolation of PCLS was performed by the combination of two procedures, as previously described [33]. PCLS were placed into MagNA Lyser Green Beads tubes (Roche Diagnostics) with 700 µl ice-cold TRIzol reagent and disrupted in a Bullet Blender Tissue Homogenizer (Next Advance). After the separation of phenol–chloroform, approx. 250 µl aqueous phase was mixed 1:1 with 75% ethanol and transferred into the Zymo-Spin IC Column from the RNA Clean & Concentrator Kit (Zymo Research). RNA clean-up and collection was done following the manufacturer's instructions.

RNA of WD-NECs was extracted using the Nucleospin RNA Plus Kit (Macherey–Nagel) according to manufacturer's protocol. For the detection of viral RNA (except H1N1) and host mRNA, the Omniscript RT kit (Qiagen) using random hexamers (Thermo Fisher Scientific) was used for reverse transcription and synthesis of complementary DNA (cDNA). Quantitative PCR (qPCR) was performed on an ABI Fast 7500 Sequence Detection System (Applied Biosystems) with target-specific primers, using the TaqMan Gene Expression Assay (Applied Biosystems) or the Fast SYBR Green Assay (Thermo Fisher Scientific). For H1N1/A/Hamburg/4/2009, one-step cDNA synthesis and qPCR were performed on a 7500 Real-Time PCR System (Thermo Fisher Scientific) using the AgPath-ID One-Step RT-PCR kit (Thermo Fisher Scientific) with target-specific primers. Results were analysed using SDS software (Applied Biosystems), with relative expression calculated using the ΔΔCT method as described [37]. Expression levels for the genes of interest were normalized to the housekeeping genes 18S ribosomal RNA (rRNA) or beta-2-microglobuline (B2M) [33, 38–47]. The sequences and concentrations of primers and probes used are listed in Table 1. For H5N1 A/turkey/Turkey/2005, the Flu panA mod primer and probes were used and for H1N1/Hamburg/4/2009, they were combined with the Flu M swine reverse primer [43].

Infectious virus titration

For IAV titration, MDCK-II cells were seeded at 10^5 cells/well density into 96-well plates and cultured overnight before infection. The virus samples were tenfold serial-diluted in serum-free growth medium, and each sample was titrated in duplicate (40 µl inoculum/well). After a 90-min adsorption at 37 °C, an overlay containing MEM with 1% (w/v) methylcellulose, 2% FBS and 1% (v/v) penicillin/streptomycin solution was added to each well (160 µl). 24 h p.i. cells were washed twice with prewarmed PBS and fixed in 4% formalin for 15 min. This was followed by two 0.1 M glycine-quench washes, and a 5-min permeabilization with 0.25% (v/v) of Triton X-100 in PBS. Primary antibody staining against viral nucleoprotein (NP) was performed using the mouse monoclonal HB-65 (ATCC, clone H16-L10-4R5) antibody diluted 1:50 in PBS, followed by the secondary antibody goat anti-mouse IgG conjugated to Alexa Fluor 488 (ThermoFisher), diluted 1:500 in PBS. Both antibodies were incubated for 1 h at 21 °C and were each followed by three washing steps with PBS. The infected cell foci were counted manually using the Observer.Z1 fluorescence microscope (Zeiss, Feldbach, Switzerland) using a 10× magnification objective, and based on this the virus titers were calculated as PFU/ml. For SARS-CoV-2 titration, VeroE6 cells were seeded at 3×10^6 cells per 24-well plate and cultured overnight before infection. The samples were diluted 1:2 and in a 1:tenfold serial dilution and added to the wells. After 1 h of incubation at 37 °C, 5% CO_2, the medium was removed and cells were overlayed with a 1:1 mix of DMEM, 20% FBS, 2X HEPES, 2X Pen/Strep and 2.4% Avicel. 48–72 h later, the overlay was removed, cells were washed with PBS, fixed in 4% formalin for 15 min, and stained with crystal violet for another 15 min. Then, wells were washed with tap water and dried before plaques were counted. Virus titers were calculated as PFU/ml.

Immunohistochemistry

Formalin-fixed PCLS were embedded in paraffin using a standard protocol by the COMparative PATHology platform (COMPATH) at the Institute of Pathology

Table 1 List of qPCR primer and probe sequences and concentrations used

Human/Viral gene	Oligo	Sequence (5′–3′)	Final conc. (nM)	Reference
18S rRNA	FW	CGCCGCTAGAGGTGAAATTC	500	[39]
	RV	GGCAAATGCTTTCGCTCTG	500	
	P	FAM-TGGACCGGCGCAAGACGGA-BHQ	125	
B2M	FW	CTCCGTGGCCTTAGCTGTG	1000	[33]
	RV	TTTGGAGTACGCTGGATAGCCT	1000	
IFN-β	FW	CGCCGCATTGACCATCTA	300	[38]
	RV	TTAGCCAGGAGGTTCTCAACAATAGTGTCA	900	
	P	FAM-TCAGACAAGATTCATCTAGCACTGGCTGGA-BHQ1	100	
IFN-λ1/IL-29	FW	GGACGCCTTGGAAGAGTCACT	300	[46]
	RV	AGAAGCCTCAGGTCCCAATTC	900	
	P	FAM-AGTTGCAGCTCTCCTGTCTTCCCCG-BHQ1	100	
IFN-λ2/3/IL-28	FW	CTGCCACATAGCCCAGTTCA	300	[46]
	RV	AGAAGCGACTCTTCTAAGGCATCTT	900	
	P	FAM-TCTCCACAGGAGCTGCAGGCCTTTA-BHQ1	100	
IP10/CXCL10	FW	CCATTCTGATTTGCTGCCTTATC	900	[40]
	RV	GCAGGTACAGCGTACAGTTCT	900	
	P	FAM-CTGACTCTAAGTGGCATTCAAGGAGTACCTCTCTC-TAMRA	100	
IL-6	FW	CCAGGAGCCCAGCTATGAAC	300	[41]
	RV	CCCAGGGAGAAGGCAACTG	900	
	P	FAM-CCTTCTCCACAAGCGCCTTCGGT-TAMRA	100	
ACE2	FW	CATTGGAGCAAGTGTTGGATCTT	1000	[44]
	RV	GAGCTAATGCATGCCATTCTCA	1000	
	P	FAM-CTTGCAGCTACACCAGTTCCCAGGCA-MGBQ500	125	
TMPRSS2	FW	Sequence information not given by the manufacturer		Applied biosystems, TaqMan gene expression assay
	RV			Hs01122322_m1
	P			
SARS-CoV-2 E Sarbeco	FW	ACAGGTACGTTAATAGTTAATAGCGT	400	Adapted from [42]
	RV	ATATTGCAGCAGTACGCACACA	600	
	P1	FAM-ACACTAGCCATCCTTACTGCGCTTCG-BBQ	125	
Flu panAmod	FW	AGATGAGYCTTCTAACCGA	500	[43]
	RV	GCAAAGACATCTTCAAGTYTC	250	
	P	FAM-TCAGGCCCCCTCAAAGCCGA-BHQ1	250	
Flu M swine	RV	GCAAAGACACYTTCCAGTCTC	250	[43]
CDK2NA (p16)	FW	TGAGCTTTGGTTCTGCCATT	1000	[47]
	RV	AGCTGTCGACTTCATGAC AAG	1000	

FW forward, *RV* reverse, *P* probe

and Institute of Animal Pathology, University of Bern, Switzerland. Briefly, PCLS were dehydrated in an ethanol series (70%, 96%, 100%, Grogg), cleared with xylol (Sigma-Aldrich), and embedded in paraffin. Using a Leica RM2135 microtome (Leica Biosystems), 7 µm thick sections were cut and mounted on glass slides (Fisherbrand Superfrost Plus, Fisher Scientific). For dewaxing, the slides were incubated at 60 °C for 1 h, followed by rehydration with three times xylol and a series of descending concentrations of ethanol (2×100%, 2×95%, 80% to 70%). For immunohistochemistry, endogenous peroxidase activity was inhibited by 3.25% H_2O_2 in 70% methanol for 10 min at room temperature followed by washing the slides in PBS. For antigen retrieval, the slides were then boiled using a microwave in 10 mM citrate buffer (pH 6.0) for two times 5 min. After washing in PBS, samples were incubated in PBS with 1% BSA (Sigma-Aldrich) for 30 min at room temperature to block nonspecific antibody binding. Then, primary antibody targeting the nucleocapsid (N) protein of SARS-CoV-2 (Rockland,

1:2′500, rabbit polyclonal IgG) in PBS with 1% BSA was incubated over night at 4 °C in a humidified chamber. After washing, slides were incubated with biotinylated goat anti-rabbit (DAKO), followed by HRP-conjugated streptavidin (DAKO), both for 10 min at room temperature protected from light, with an interposed washing step. Next, slides were washed in PBS and AEC-substrate chromogen was incubated for 10 to 15 min at room temperature. Then, slides were washed in tap water, followed by distilled (d)H_2O and hematoxylin staining of the nuclei for 2 min. Afterwards, slides were again washed in tap water followed with dH_2O. Slides were then covered with Aquatex mounting media (Merck) and a coverslip.

Immunofluorescence

After 24 h, formalin-fixed PCLS were washed twice with PBS and stored in 70% ethanol at 4 °C, until further processing. For staining, the ethanol was removed by three 10-min washes in PBS at room temperature. Permeabilization was done with PBS-Triton X-100 0.3% supplemented with 2% BSA for 15 min at room temperature. Blocking was then performed with PBS-Triton X-100 0.3% supplemented with 30 mg/ml milk powder and 10% FBS (blocking solution), for 1 h at room temperature. Primary antibody against advanced glycosylation end-product specific receptor (AGER, R&D Systems, 1:250), pro-surfactant protein C (pro-SFTPC, Novus Biologicals, 1:800), IAV nucleoprotein (NP, 1:50), and SARS-CoV-2 nucleocapsid protein (N, clone E16C, Fisher Scientific, 1:25) were diluted in blocking solution and then added and incubated overnight at 4 °C. This was followed by three 10-min washes in PBS-Triton 0.1% at room temperature. Finally, the secondary antibody donkey anti-goat IgG (1:400, AGER) or goat anti-rabbit IgG (1:400, pro-SFTPC), both conjugated to Alexa Fluor 546, goat anti-mouse IgG (1:500, IAV) or goat anti-mouse IgG2b (1:250, SARS-CoV-2), both conjugated to Alexa Fluor 488, Phalloidin conjugated to Alexa Fluor 546 (1:100, for IAV staining only), and DAPI staining at 1:1000 dilution, in blocking solution was added to the PCLS and incubated for 5 h at 4 °C. The samples were mounted on glass slides using the EMS Shield Mount with DABCO (AGER and pro-SFTPC, EMS, USA), ProLong Gold antifade reagent (IAV, Fisher Scientific), or Mowiol (SARS-CoV-2, Merck/Calbiochem). All the incubations and washing steps were performed under soft rocking for better results. The imaging was performed using the Nikon confocal A1 microscope (IAV NP, Phalloidin) or by laser scanning confocal microscopy using Olympus FV3000 with FluoView FV3000 system software (SARS-CoV-2 N, AGER, pro-SFTPC) and Zeiss LSM 710 (AGER, pro-SFTPC). Images were processed and rendered in the Nikon NIS Elements Confocal version 4.30 software (IAV) and Fiji, or ImageJ image processing package v1.54f or v1.53q, respectively (SARS-CoV-2, AGER, pro-SFTPC).

Cytotoxicity assay

Lactate dehydrogenase (LDH) release was assessed in the supernatants (four technical replicates per sample) of Mock-, SARS-CoV-2-, and IAV-infected PCLS using the CytoTox 96 Non-Radioactive Cytotoxicity Assay (Promega) following manufacturer's instructions. Absorbance was measured at 490 nm with the Biotek 800 TS absorbance reader (Agilent technologies). To calculate the percentage of cytotoxicity, growth medium background was subtracted and resulting values were divided by the maximum LDH release, which was obtained by taking the supernatant of PCLS, treated with 2% Triton X-100 (Merck) for 4 h at 4 °C.

Immunoassay

In supernatants harvested 48 h p.i., protein levels of type I (beta) and type III (lambda 1/3) interferons (IFNs) and interleukin 6 (IL-6), as well as IFN gamma-induced protein 10 (IP10/CXCL10) were measured with the DuoSet ELISA kits (R&D Systems) following manufacturer's instructions. Absorbance was measured at 450 nm with the Biotek 800 TS absorbance reader (Agilent technologies).

Statistical analysis

Statistical analysis was performed using GraphPad Prism v9 and v10. The specific statistical tests used are indicated in the figure legends.

Results

PCLS cultures from aged lungs present a senescent phenotype

To investigate the impact of aging on respiratory virus infection, lung tissue from donors with ages ranging from 36 to 81 years old were used to generate PCLS cultures (Fig. 1A and Table 2). PCLS retained the native microstructure and cellular composition of the alveolar epithelium, as confirmed by staining for the advanced glycosylation end-product specific receptor (AGER), which is expressed at high baseline levels primarily in alveolar type 1 cells [48], and for pro-surfactant protein C (SFTPC), a marker for alveolar type 2 cells (Fig. 1B, C). Further, we observed a significant association between tissue donor age and mRNA levels of the senescence marker *CDKN2A* (p16), indicating higher frequency of senescent cells in PCLS obtained from older donors (Fig. 1D).

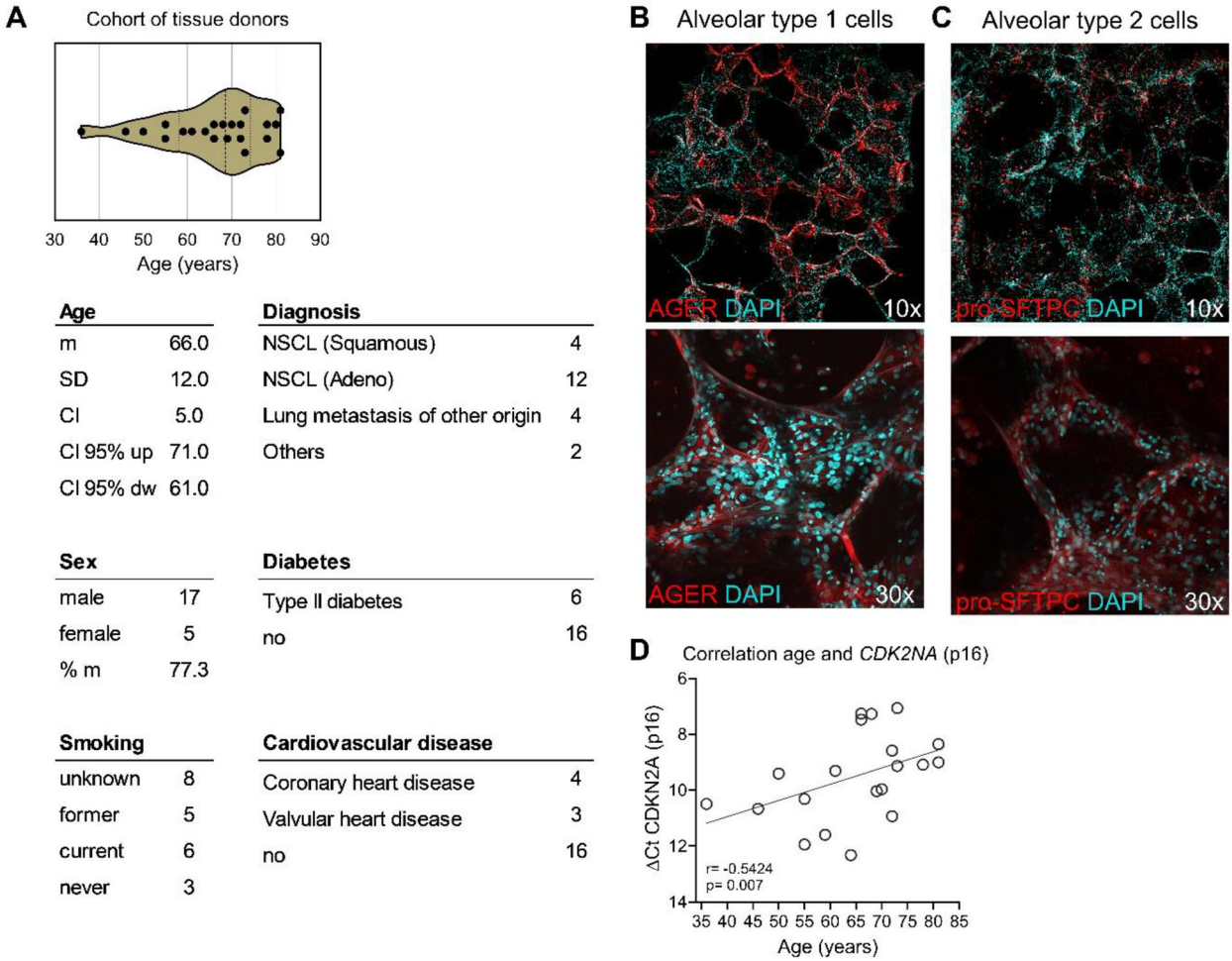

Age	
m	66.0
SD	12.0
CI	5.0
CI 95% up	71.0
CI 95% dw	61.0

Diagnosis	
NSCL (Squamous)	4
NSCL (Adeno)	12
Lung metastasis of other origin	4
Others	2

Sex	
male	17
female	5
% m	77.3

Diabetes	
Type II diabetes	6
no	16

Smoking	
unknown	8
former	5
current	6
never	3

Cardiovascular disease	
Coronary heart disease	4
Valvular heart disease	3
no	16

Fig. 1 PCLS cultures from aged lungs present a senescent phenotype. **A** Violin plot representing the age distribution of the individual donors used for the generation of the PCLS cultures. The dashed vertical line indicates the median value, whereas the dotted lines indicate the interquartile ranges. Each symbol represents an individual donor. The table summarizes patient's characteristics: age (mean, m; standard deviation, SD; confidence interval, CI; down, dw), sex (% male, m), smoking status (n), diagnosis, and other comorbidities, specifically diabetes and cardiovascular disease. **B**, **C** Representative confocal microscopy evaluation of PCLS stained for **(B)** AGER, highly expressed in alveolar type 1 cells, or **(C)** the alveolar type 2 cell marker pro-SFTPC. Micrographs are projections of 3D captures. Magnification 10X and 30X. AGER and pro-SFTPC, red; DAPI, light blue. **D** Correlation of deltaCt *CDKN2A* (p16) (deltaCt = Ct CDKN2A-Ct B2M) and donor age. Association was tested using the one-tailed Spearman rank correlation test, whereas the correlation coefficient (r) is given and a p value lower than 0.05 (*), 0.005 (**), 0.0005 (***), 0.0001 (****) is significant. Each symbol represents an individual donor

Human PCLS are productively infected by pandemic and avian IAV strains

We first studied the effect of age on IAV infection using pandemic H1N1 and avian H5N1 strains. Specifically, we infected PCLS from three and four donors (64, 72, 81 and 36, 73, 78, 81 years old, respectively) with 10^6 PFU of A/Hamburg/4/2009 (H1N1) or A/turkey/Turkey/2005 (H5N1), respectively. Two h p.i., PCLS were washed twice and incubated at 37 °C for 4 to 72 h. To preserve tissue viability, culture medium was changed every day, and at selected time points p.i., individual PCLS from the same donor were harvested for further analysis (Fig. 2A).

Immunofluorescence analysis using the cytoskeleton component F-actin indicated a preserved alveolar microstructure, both in non-infected controls (Mock) and IAV-infected PCLS at all the time points p.i. analyzed (Fig. 2B). Furthermore, the frequency of IAV NP-positive cells increased over time and individual NP-positive cells, as well as foci of infected cells, spread within the PCLS, suggesting productive IAV replication (Fig. 2B). Accordingly, infectious titers in the tissue culture supernatant were low at 4 h p.i. but increased in the following time reaching a maximum of about 10^5 PFU/ml at 24 h p.i. (Fig. 2C). Notably, H1N1 replicated in human PCLS

Table 2 Characteristics of the pulmonary tissue donors

No	Age	Sex	Smoking status	Diagnosis	Diabetes	CVD
1	81	Male	Unknown	NSCL (Squamous Ca)	type II	Coronary heart disease, arrhythmia
2	72	Male	Unknown	NSCLC (Adeno Ca)	No	No
3	66	Male	15 py, former smoker	NSCLC (Adeno Ca)	No	No
4	50	Female	Most probably never smoker	Lung metastasis of Melanoma	No	No
5	55	Male	50 py, smoker	NSCLC (Adeno Ca)	No	No
6	68	Female	Unknown	NSCLC (Adeno Ca)	No	No
7	70	Male	Unknown	NSCLC (Adeno Ca)	No	No
8	55	Male	35 py, smoker	Benign (lymphocytic nodule)	No	No
9	59	Male	Undetermined py, current smoker	NSCLC (Adeno Ca)	No	No
10	46	Male	25 py, current smoker	Lung metastasis of Ca of testicle	No	No
11	69	Male	30py, former smoker	NSCLC (Squamous Ca)	No	No
12	66	Male	30 py	NSCLC (Adeno Ca)	No	No
13	61	Male	22 py, stopped 2018	NSCLC (Adeno Ca)	Type II	No
14	73	Male	60 py, stopped 2021, now e-cigarettes	NSCLC (Squamous Ca)	Type II	No
15	36	Male	Unknown	Lung metastasis of colon Ca	No	No
16	81	Male	Never smoker	NSCLC (Adeno Ca)	No	Coronary heart disease, valvular heart disease
17	72	Female	Unknown	Atypical carcinoid	Type II	Hypertensive and valvular heart disease
18	64	Female	Unknown	NSCLC (Adeno Ca)	No	No
19	73	Female	20 py, stopped 19 years ago	NSCLC (Adeno Ca)	No	No
20	78	Male	Unknown	Lung metastasis of Melanoma	No	Hypertensive and valvular heart disease
21	78	Male	Never smoker	NSCLC (Adeno Ca)	Type II	Coronary heart disease
22	80	Male	60 py	NSCLS (Squamous Ca)	Type II	coronary Heart disease

Ca carcinoma, *NSCLC* Non-small cell lung cancer, *py* pack-years, *CVD* cardiovascular disease

in the absence of exogeneous trypsin, indicating that cellular proteases were present that cleaved the H1N1 hemagglutinin (HA) at the monobasic cleavage site [49–51]. While tissue-associated viral RNA levels for H1N1 reached highest levels 24 h p.i. and remained high, viral RNA levels for H5N1 decreased about 1–2 logs from 24 to 72 h p.i. in PCLS from all the four donors (Fig. 2D). Of note, RNA levels of H1N1 and H5N1 cannot be compared to each other due to distinct qPCR assays used. For further correlation analysis, we used tissue-associated viral RNA levels which, in contrast to live virus release, can be normalized to the cell number within the tissue using the housekeeping 18S rRNA. Overall, viral RNA loads for both, H1N1 and H5N1, were significantly lower in aged tissue as shown in relation to donor age as well as to the expression of the senescence marker p16, indicating that aging lung cells do not provide an optimal replication environment for IAV (Fig. 2E, F).

Low level of SARS-CoV-2 replication in human PCLS

Next, we investigated if this age-effect towards IAV replication was also observed with another significant respiratory virus, SARS-CoV-2. Entry into target cells is mediated through binding of the viral trimeric spike protein to the cell surface receptor angiotensin-converting enzyme 2 (ACE2) after priming by transmembrane protease serine subtype 2 (TMPRSS2) [52–54]. Thus, expression of ACE2 and TMPRSS2 mRNAs in PCLS was confirmed in selected donors. However, ACE2 mRNA levels were found to be lower in PCLS compared to primary human nasal epithelial cells (Fig. 3A). Next, using an early clinical isolate of SARS-CoV-2 (München1.1/2020/929, "Early isolate") and the VOC SARS-CoV-2 Delta, infection experiments were performed on PCLS generated from a cohort of donors of various age (36–81 years old). PCLS were exposed to 10^6 PFU of SARS-CoV-2 and processed as illustrated in Fig. 3B. Immunohistochemistry and immunofluorescence analysis revealed foci of infection at different structural localizations, suggesting a variable cell tropism of SARS-CoV-2 (Fig. 3C, D). In contrast to the high titers measured for IAV-infected PCLS, both SARS-CoV-2 Early and Delta isolates, replicated to lower levels, peaking at around 10^3 PFU/ml (Fig. 3E). Whole genome sequencing of both isolates confirmed the absence of deletions or mutations at the spike polybasic cleavage site, which might impair viral replication [36]. While 40% of the Early isolate have a 686S, there is a mutation

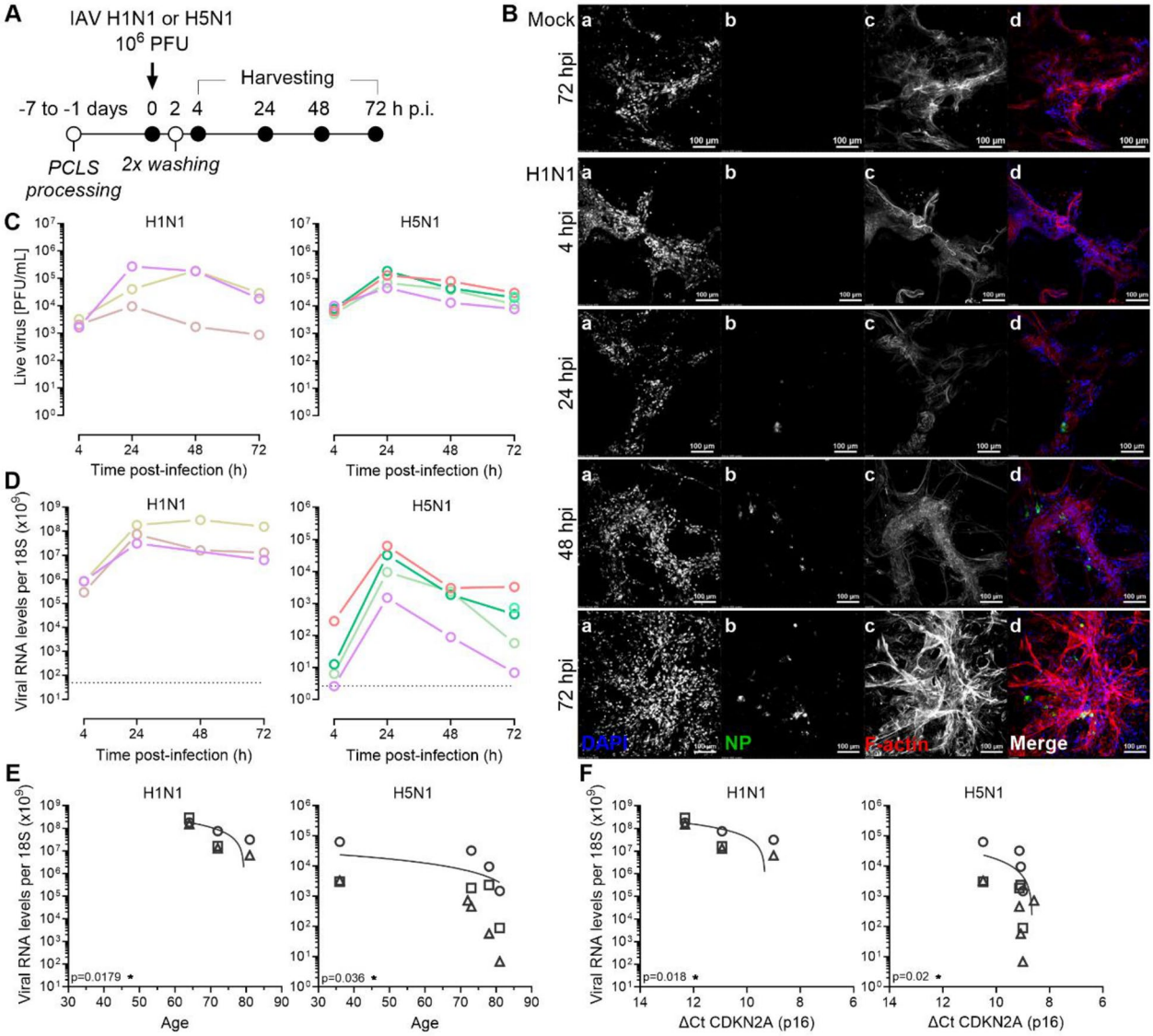

Fig. 2 Human PCLS are productively infected by pandemic and avian IAV strains. **A** PCLS were infected one to seven days after generation with 10^6 PFU of IAV H1N1 A/Hamburg/4/2009 or H5N1 A/turkey/Turkey/2005. After 2 h PCLS were washed twice with PBS. Culture medium was changed daily. 4, 24, 48, and 72 h p.i. supernatants and PCLS were harvested for further analysis. **B** Representative confocal microscopy evaluation of Mock- and H1N1-infected PCLS, 4, 24, 48, and 72 h p.i. a, DAPI; b, IAV nucleoprotein (NP); c, F-actin; d, merge: DAPI, blue; IAV NP, green; F-actin, red. Scale bars, 100 µm. **C** Supernatants of infected PCLS were analyzed with a PFU assay. Each line represents an individual donor. **D** Tissue-associated viral RNA loads per 18S rRNA in PCLS over time following IAV infection. Dotted line represents the detection limit. **E** Correlation of tissue-associated viral RNA and donor age. **F** Correlation of tissue-associated viral RNA and deltaCt *CDKN2A* (p16) (deltaCt = Ct CDKN2A-Ct B2M). Association was tested using the Spearman rank correlation test. Each symbol represents an individual donor at 24 h (circle), 48 h (square), or 72 h p.i. (triangle). IAV H1N1, n = 3 and H5N1, n = 4

in 50% leading to a S686G amino acid change. The Delta isolate has the expected variant defining mutation leading to P681R [55] (Fig. S1A). Furthermore, we assessed extracellular viral RNA of 14 PCLS donors infected with SARS-CoV-2 Early isolate and found notable levels at different timepoints p.i. (Fig. 3F). Overall, tissue-associated viral RNA levels increased during 24 to 48 h p.i. for SARS-CoV-2 Early isolate-infected PCLS. After 48 to 72 h p.i., we could observe a plateau or slightly decreasing levels for most donors and of about 1.6 to 2 logs in three out of 14 donors (Fig. 3G). Interestingly, within 48 h p.i. Delta isolate-infected PCLS showed an increase in tissue-associated viral RNA of about one to two logs for most donors tested. Thereafter, a plateau was reached too

(Fig. 3G). Furthermore, for SARS-CoV-2 Early isolate-infected PCLS, significantly lower viral RNA levels with increasing donor age as well as with increasing *CDK2NA* (p16) expression were measured. For Delta-infected PCLS we could observe a trend towards lower viral RNA levels with increasing age and senescence marker *CDKN2A* (p16). Altogether, our data indicate that aged/senescent PCLS are less permissive to SARS-CoV-2 replication (Fig. 3H, I). Furthermore, elevated ACE2 mRNA levels were correlated with increased p16 expression but showed no association with older age (Fig. S2A). Finally, ACE2 gene expression did not change upon SARS-CoV-2 infection, an observation reported as well by others (Fig. S2B) [18]. In summary, PCLS generated from lungs of older compared to younger individuals are less susceptible to SARS-CoV-2 infection, a feature that among other factors, might be related to CDK2NA (p16) levels but independent of the ACE2 cell-surface receptor.

IAV induces cytotoxicity and a robust pro-inflammatory response in human PCLS

To investigate the impact of viral infection on the viability of lung tissue, we evaluated cytotoxicity using a LDH assay. Avian H5N1 IAV and SARS-CoV-2 Early isolate infections led to elevated release of LDH after 72 or 48–72 h p.i., respectively. While in comparison to Mock, avian H5N1 IAV infection led to elevated, although not significant, release of LDH ($p = 0.07$), there was little cytotoxicity upon H1N1 pandemic IAV or SARS-CoV-2 infection (Fig. 4A, Fig. S3A). Of note, there was no association of cytotoxicity with donor age (Fig. S4A). Considering the robust inflammatory responses induced by IAV and SARS-CoV-2 infections in vivo [56–63], we evaluated the pro-inflammatory and antiviral responses of PCLS following infection with both viruses. To do so, we measured the mRNA and protein levels of type I (beta) and type III (lambda 1/3) IFNs and IL-6, as well as IP10/CXCL10. Up to 72 h p.i. with SARS-CoV-2 (both Early as well as Delta isolates), there was limited induction of IFNs, both at the mRNA and protein levels (Fig. 4B, C Fig. S3B, C), most likely reflecting the low level of SARS-CoV-2 replication in PCLS (Fig. 3E, F, G). On the other hand, H1N1-infected PCLS revealed a tendency towards higher IFN mRNA levels and avian H5N1 infection induced significant IFN responses as early as 24 h p.i. Specifically, in comparison to Mock-infected PCLS, H5N1 induced about one log, three logs, and four logs higher mRNA expression levels of IFN-β, IFN-λ1, and IFN-λ2/3, respectively (Fig. 4B, Fig. S3D, E). In line, H1N1 infection led to the release of IFNs in one out of two donors measured, and H5N1 infection induced significant release of both, IFN- β and IFN-λ1/3. This is also in line with rapid virus replication and high viral RNA levels for H5N1 24 h p.i. (Fig. 2C, D). In addition, the early and remarkable antiviral response might explain the rapid decrease of H5N1 viral RNA thereafter, 48 to 72 h p.i. (Fig. 2D). The mRNA level of IFN-λ2/3 was notably positively correlated with donor age in SARS-CoV-2 Early isolate-infected PCLS, but not in other conditions. This suggests that the early, non-human-adapted variant of SARS-CoV-2 may have had a less efficient mechanism for evading the IFN system (Fig. S4B-E). Compared to Mock and SARS-CoV-2 Early isolate, Delta isolate-infected PCLS showed a trend toward higher mRNA and protein levels of IL-6 and IP10/CXCL10, although this difference was not statistically significant. This is likely due to the small sample size and variability, even within the Mock condition. A similar tendency in terms of IL-6 induction was observed for H1N1-infected PCLS. In contrast, H5N1 infection induced significant IL-6 expression on mRNA and protein levels 72 h p.i. and 48 h p.i, respectively. Notably, both IAV strains led to significant induction of IP10/CXCL10 expression

(See figure on next page.)

Fig. 3 SARS-CoV-2 infection of human PCLS is leading to a low level of replication. **A** ACE2 and TMPRSS2 mRNA levels per 18S rRNA in PCLS of selected donors. Boxplots indicate the median value (centerline) and interquartile ranges (box edges), with whiskers extending to the lowest and the highest values. (ACE2, n = 15; TMPRSS2, n = 4). Fold difference was calculated by comparing the median ACE2 expression of all the PCLS (n = 15) and WD-NEC (n = 3) donors tested. **B** PCLS were infected one to seven days after generation with 10^6 PFU of SARS-CoV-2 (SARS-CoV-2/München1.1/2020/929; Early isolate) and Delta isolate (Delta AY.127, hCoV-19/Switzerland/BE-IFIK-918–4879/2021). After 2 h PCLS were washed twice with PBS. Growth medium was changed daily. 4, 24, 48, and 72 h p.i. supernatants and PCLS were harvested for further analysis. **C** Histological section of a representative Mock- and SARS-CoV-2 Delta isolate-infected PCLS 48 h p.i., stained for the nucleocapsid (N) protein and counterstained for hematoxylin. **D** Representative confocal microscopy evaluation of Mock- and SARS-CoV-2 Early isolate-infected PCLS 48 h p.i., stained for DAPI (grey) and SARS-CoV-2 N protein (green). a, Mock; b-e, SARS-CoV-2 Early isolate-infected PCLS. a-c, micrographs are projections of 3D captures. a-e, magnification 10X. **E** Supernatants of infected PCLS were analyzed with a PFU assay. Early isolate, n = 18; Delta isolate, n = 7. **F** Extracellular viral RNA in the supernatant of SARS-CoV-2 Early isolate-infected PCLS over time expressed as viral RNA copies per ml (n = 14). **G** Tissue-associated viral RNA loads per 18S rRNA in PCLS over time following SARS-CoV-2 infection. Dotted line represents the detection limit. Early isolate, n = 15; Delta isolate, n = 7 **H** Correlation of tissue-associated viral RNA and donor age. **I** Correlation of tissue-associated viral RNA and deltaCt *CDKN2A* (p16) (deltaCt = Ct CDKN2A-Ct B2M). Association was tested using the Spearman rank correlation test. Each symbol represents one individual donor at 24 h (circle), 48 h (square), or 72 h p.i. (triangle)

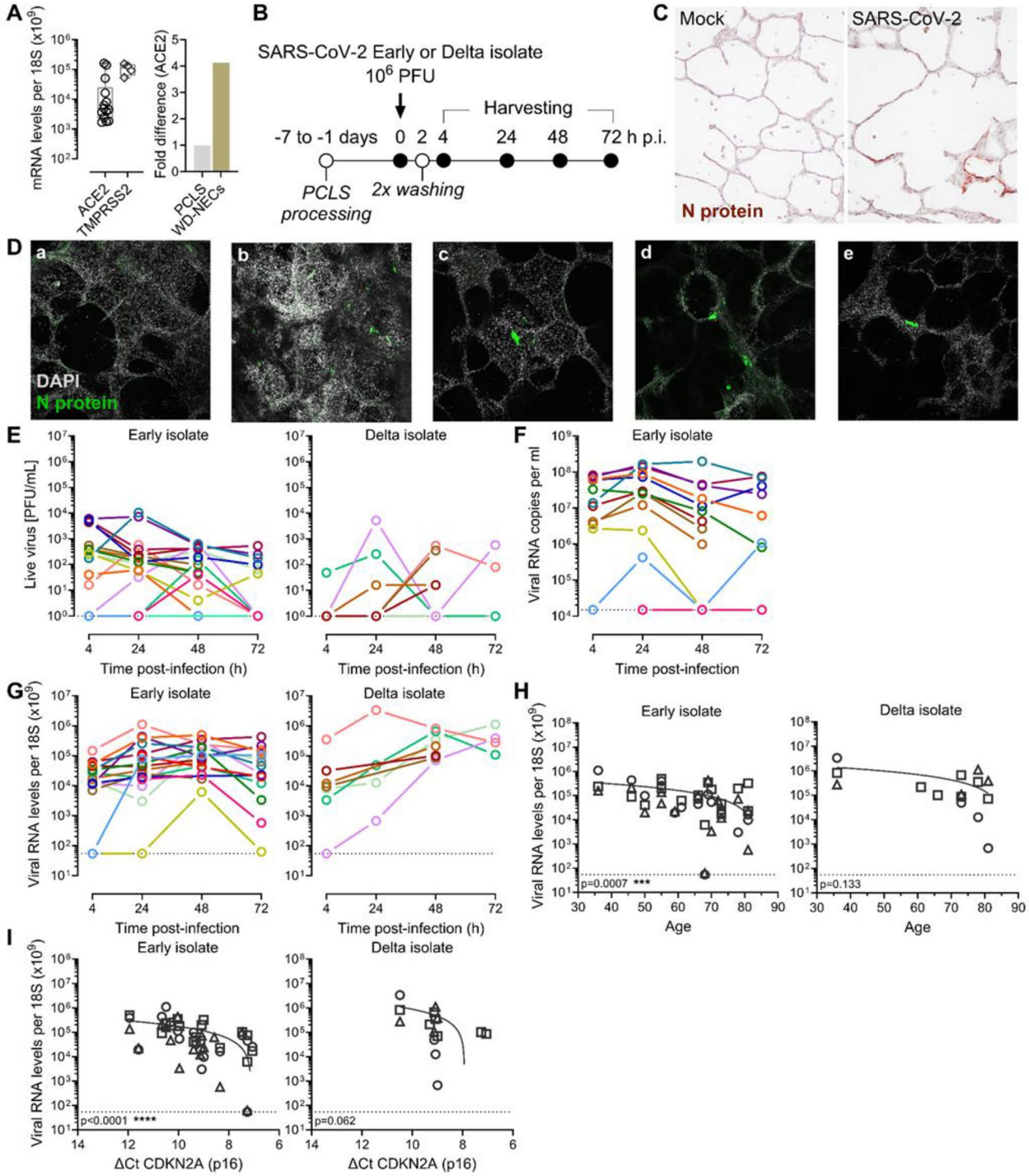

Fig. 3 (See legend on previous page.)

as early as 24 h p.i. (Fig. 4D, E, Fig. S3B-E). With the exception of H1N1-infected PCLS, where higher IP10/CXCL10 mRNA levels were associated with older donor age, no correlation was observed between donor age and mRNA levels of IL-6 or IP10/CXCL10 in other conditions (Fig. S4B-E). Altogether, SARS-CoV-2 is less cytotoxic and a weaker inducer of pro-inflammatory mediators compared to IAV H5N1.

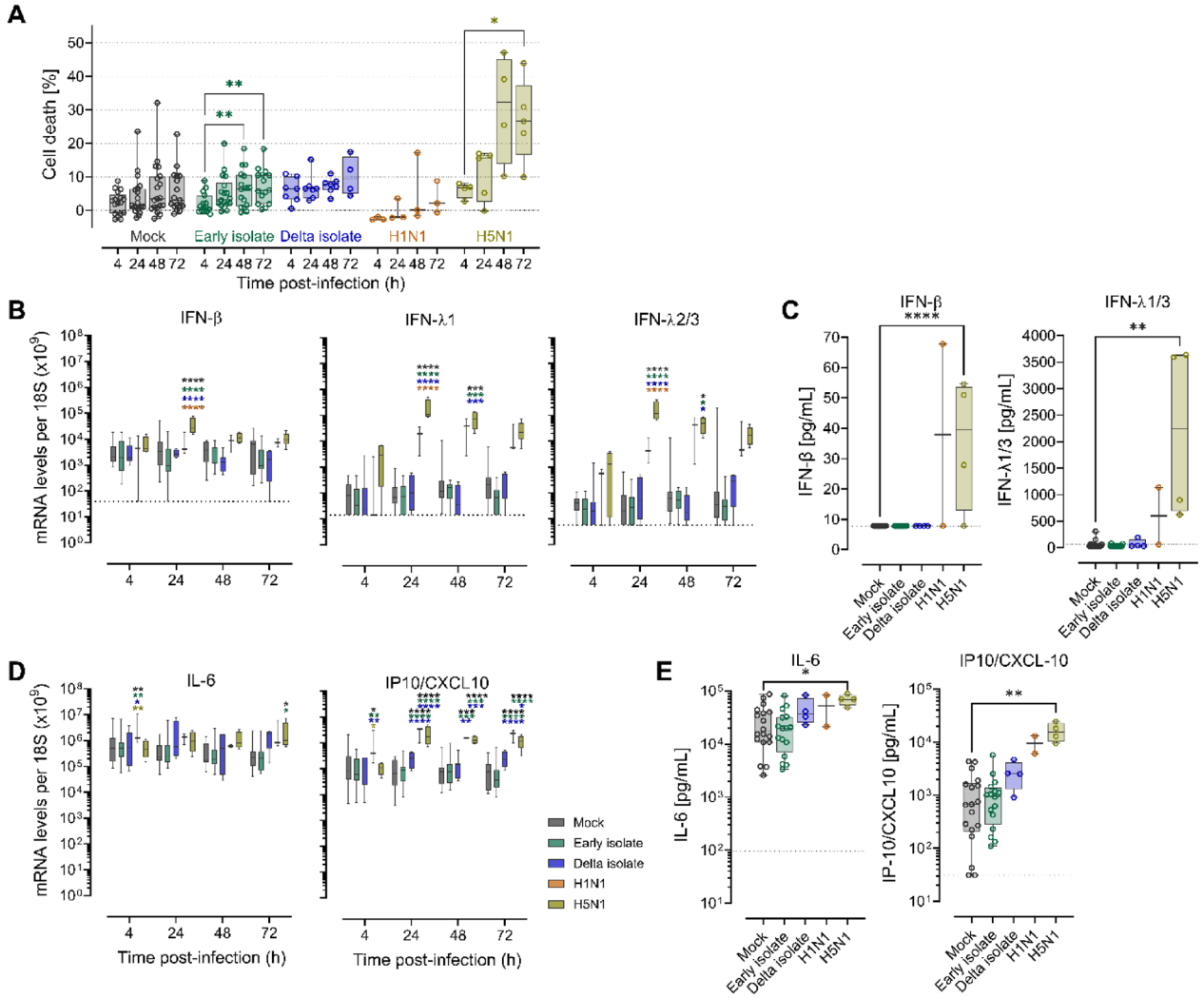

Fig. 4 IAV is cytotoxic and induces a robust pro-inflammatory response in human PCLS. **A** Cell death (%), calculated from lactate dehydrogenase (LDH) release in PCLS, exposed to 10^6 PFU of SARS-CoV-2 Early or Delta isolate, and IAV H1N1 or H5N1 over time. A two-way ANOVA and Tukey's multiple comparisons test was applied to compare the different groups to Mock (not significant) and the different timepoints of a group to its 4 h p.i. timepoint. Each symbol represents an individual donor. **B** IFN-β, IFN-λ1, IFN-λ2/3 and **(D)** IL-6, IP10/CXCL10 mRNA expression levels per 18S rRNA over time. A two-way ANOVA and Tukey's multiple comparisons test was applied to compare the different groups. **C** IFN-β and IFN-λ1/3, and **E** IL-6 and IP10/CXCL10 protein levels in supernatants harvested 48 h p.i. in pg/ml. A Kruskal–Wallis test with Dunn's multiple comparisons test was applied to compare infection groups to Mock. The dotted line represents the detection limit of the assays. Mock, black; SARS-CoV-2 Early isolate, green; SARS-CoV-2 Delta isolate, blue; IAV H1N1, orange; IAV H5N1, yellow. Boxplots indicate the median value (centerline) and interquartile ranges (box edges), with whiskers extending to the lowest and the highest values

Discussion

In this study, we explored the impact of donor age on the susceptibility of the human distal lung epithelium to respiratory virus infection. To do so, we used an ex vivo model based on PCLS cultures prepared from lung tissue of individuals spanning from 36 to 81 years of age. Our data demonstrate that tissue donor age is associated with distinct susceptibility of PCLS to IAV and SARS-CoV-2 infection, with PCLS from older versus younger donors being less permissive to both viruses. Furthermore, while SARS-CoV-2 infection was leading to little cell death and triggered only limited host responses, IAV infection, especially H5N1, caused more cytotoxicity and robust pro-inflammatory responses.

The differential replication potentials in the distal lung, high for several IAV strains and low for SARS-CoV-2 variants, have been previously documented using unprocessed lung explants and PCLS [16–18, 21]. In contrast, when comparing donors of different ages, PCLS offer greater homogeneity and reproducibility compared to

unprocessed lung explants. This is due to the precision in cutting and the ability to generate consecutive slices from the same lung biopsy, which reduces variability between sample replicates. However, the availability of human lung tissue is limited, which in turn restricts the number of experimental conditions that can be tested. Regarding the experimental size, due to recruitment limitations, less lung tissue from patients with young age could be obtained. While SARS-CoV-2 Early and Delta isolates replicated at low levels in PCLS, IAV H1N1 and H5N1 replication resulted in the release of significant amounts of infectious viral particles into the culture supernatant. The disparate susceptibility of PCLS to SARS-CoV-2 and IAV infection is possibly due to differences in the alveolar cell surface expression of cognate virus receptors. For instance, ACE2 expression was lower in PCLS compared to WD-NEC cultures and has been shown to gradually decrease from the upper to the lower human respiratory tract and thereby relating to virus infectivity [64]. A similar coherence of receptor expression levels and susceptibility to SARS-CoV-2 infection was recently reported for human placenta explants [65]. Furthermore, using a high-sensitivity RNA in situ mapping approach, ACE2 was revealed to be expressed in less than 1% of alveolar type 2 cells [64, 66, 67]. In alveolar organoids, Hönzke et al. showed limited permissiveness of the human distal lung for SARS-CoV-2 infection due to sparse ACE2 levels and that viral replication can be increased by ACE2 overexpression [18]. Nevertheless, SARS-CoV-2 infection of the lower respiratory tract was shown in pathological samples of COVID-19 patients [68, 69]. The virus likely reaches the distal lung via droplets aspiration from the naso- and oro-pharynx, although the exact mechanisms are unknown. In contrast, the HA of IAV primarily binds to sialic acid residues (SA, *N*-acetylneuraminic acid), that are part of cell surface glycoconjugates which mediate virus attachment to the host cell [70]. The binding of human and avian IAV to SA in α2,6- and α2,3-glycosidic linkage, respectively, is believed to be an important species barrier [71–73]. While SAα2,6 residues are abundantly expressed on airway cells throughout the conducting airways [74, 75], SAα2,3 residues are predominantly expressed by alveolar type 2 cells and resident macrophages of the distal lung and less abundantly expressed in the human upper respiratory tract. Accordingly, avian IAV was shown to replicate efficiently in the lower respiratory tract while replication in the upper respiratory tract is very limited [71–73]. Consequently, human-to-human transmission of avian IAV such as the highly pathogenic H5N1 is rare [76]. Still, H5N1 IAV is a prevailing pandemic threat and led to 882 confirmed cases between 2003 and 2023, with a case fatality rate as high as 52% [77].

Interestingly, for all viruses tested, we found an association of lower viral RNA levels with older age of the tissue donor and with higher *CDK2NA* (p16) expression levels. Generally, association of viral load dynamics with age is highly debated in literature. Whereas in some studies no differences in SARS-CoV-2 RNA loads between children and adults were found [78, 79], others reported slightly lower viral RNA loads in children [80, 81]. Furthermore, ACE2 expression was shown to be age-dependent in the nasal epithelium [82] as well as in alveolar type 2 cells [83], with lower expression in children compared to adults. However, our study focused on lung tissue from adult donors and didn't include younger adults and children. Nevertheless, no correlation of ACE2 expression and donor age was found. This is in line with another study, where no differences in ACE2 transcript levels in lung samples from deceased humans of different age were found [84]. Furthermore, senescence has been reported to lead to enhanced expression of ACE2 in primary human small airway epithelial cells, when treated with condition media of senescent cells [13]. In line, we found that higher ACE2 expression correlated with higher *CDK2NA* (p16) expression levels. Since senescent cells accumulate with age and have other potentially adverse functions, this phenomenon might explain why the elderly are more susceptible to severe COVID-19 [85]. However, the interplay between viruses and cellular senescence is complex. In some cases, virus infection can induce cellular senescence and subsequently restrict or improve virus propagation, while in others, certain viruses evolved strategies to subvert senescence [86]. Moreover, it should be pointed out that most of the recruited donors presented tobacco use history. While only six were current smokers at the time of tissue gathering, the smoke exposure could have influenced the ACE2 expression [87–89]. However, due to limited sample size considering the number of variables related to donors' tobacco use history (packs per year, for how long former smokers stopped smoking, unknown status), no further analysis could be made in line with the current study. In contrast to a previous study on IAV-induced senescence [12], we observed lower viral loads in the aged pulmonary tissue for all the IAV strains and SARS-CoV-2 isolates tested. Nevertheless, using comprehensive approaches to analyze autopsy-derived lung specimens of patients with COVID-19 in comparison to age-matched control individuals, Wang et al. identified parenchymal lung senescence as a contributor to COVID-19 pathology [90]. Thus, illustrating the limitations of ex vivo models, acute infection of PCLS might not reflect the effect of virus infection on senescence and vice versa. However, specific characteristics of senescence are cell type specific and thus would require in-depth analysis using

for example single-cell RNA sequencing, proteomics, or related approaches [91, 92], whereas many of those are already established for the PCLS model [93].

Several studies have demonstrated that H5N1 infection leads to a more robust induction of cytokines and chemokines compared to H1N1 [94–98]. Furthermore, H5N1 infected humans present unusually high serum concentrations of pro-inflammatory cytokines and chemokines, which are believed to contribute to disease severity [60–62, 99]. Similarly, characteristic features of severe COVID-19 are the excessive release of pro-inflammatory cytokines, a so-called "cytokine storm", and an immune dysregulation, specifically, a massive immune stimulation resulting in a macrophage activation syndrome, aberrant neutrophil activation, or T cell hyperreactivity. Notably, the most destructive phase of immune-driven pathogenesis often happened when the viral RNA was no longer detectable [56, 100–103]. However, our experimental set up only reflects the acute phase of infection and not what happens in vivo one to two weeks post infection. Nevertheless, a previous study using PCLS, revealed down-regulation of type I IFN-related genes at various timepoints post-SARS-CoV-2-infection, indicating a potential role of this pathway in disease progression [21]. In line, we observed very limited IFN-β mRNA and no protein response following SARS-CoV-2 infection. SARS-CoV-2 infection of PCLS did not lead to significant induction of IL-6 or IP10/CXCL10 expression, indicating that the local cellular environment alone, independent of circulating immune cells, cannot cause the massive local cytokine production seen in severe COVID-19 cases. Nevertheless, Delta isolate-infected PCLS revealed a trend towards increased IL-6 and IP10/CXCL10 mRNA and protein levels, although no statistical significance is reached, most likely due to the limited number of donors. In contrast, following SARS-CoV-2 infection of PCLS originating from anonymous tissue donors, Pechous et al. found significant induction of IP10/CXCL10 at protein level, whereas no details about tissue condition and donor comorbidities are known. Although edges of tumor resections are commonly used as a control, some genes in these areas could be affected by the tumor milieu and might influence our results [104–106]. Furthermore, culture conditions influence the innate immune response of PCLS. Thereby, supplementation of culture medium with FBS induces a higher cytokine response in comparison to serum free medium, possibly due to higher fibroblast proliferation under FBS high conditions [107]. Therefore, we used low FBS levels and it's important to mention that our PCLS were incubated in culture medium for one to seven days before infection, to minimize procedural stress and prevent the potential activation of pro-inflammatory mechanism. In the same study, IL-6 was shown to be constitutively released from non-infected PCLS, which is in line with our results from Mock-treated PCLS, indicating no pre-activation of our PCLS [21]. On the other hand, H5N1 and to lesser extent H1N1 induced significant IL-6 and IP10/CXCL10 expression and higher cytotoxicity levels, suggesting a contribution of the alveolar epithelium in the overexuberant inflammatory responses observed in severe IAV cases. The differences in host response observed between SARS-CoV-2- and IAV-infected PCLS likely also reflect the distinct viral replication profiles. Additionally, our results suggest that the pulmonary environment remains immunocompetent throughout all ages tested. Even though there are some limitations, the PCLS model is obviously purposeful to analyze certain questions independent of circulating immune cells. Furthermore, PCLS offer an ex vivo platform for antiviral drug testing or screening for senolytic drugs, either during acute infectious lung diseases or independently of infection, using tissue from donors across various age groups. The advantages of this model for testing drug efficacy, were nicely shown before, for an antiviral agent inhibiting not only viral replication but also production of pro-inflammatory cytokines [21].

In summary, our data show that pulmonary tissues from older donors are generally less susceptible to IAV and SARS-CoV-2 replication compared to those from younger donors. Unlike SARS-CoV-2, IAV replicated more efficiently in the human alveolar epithelium, triggering stronger innate immune responses. Our findings suggest that the increased risk of severe disease in the elderly is not solely due to greater local viral replication but may involve other mechanisms, such as immune-mediated pathogenesis.

Supplementary Information

The online version contains supplementary material available at https://doi.org/10.1186/s12931-025-03190-0.

Additional file 1: Fig. S1: Whole genome sequencing of SARS-CoV-2 Early and Delta isolates. A graphical overview of the SARS-CoV-2 whole genome with particular focus on the sequence of the polybasic cleavage site of the spike protein. Whole-genome sequencing analysis was done using Nanopore sequencing technology. Consensus sequences of Wuhan-Hu-1 and the virus stocks of the Early and Delta isolates were aligned, whereas the Wuhan sequence was used as a reference sequence. The amino acid change of Spike S686S/G in the Early isolate is due to a polymorphism of A to G, whereas 50% of the nucleotides at the genome position 23618 were G. The amino acid change in Spike P681R of the Delta isolate is a variant defining mutation of Delta. Fig. S2: Association of higher ACE2 expression with elevated CDK2NAlevels. (**A**) Correlation of ACE2 mRNA levels per 18S rRNA in non-infected PCLS, 24 h p.i. and donor age or deltaCt *CDKN2A* (p16) (deltaCt = Ct CDKN2A-Ct B2M). (**B**) Correlation of ACE2 mRNA and viral RNA per 18S rRNA in SARS-CoV-2 Early isolate-infected PCLS 24 h p.i. Association was tested using the Spearman rank correlation test. Each symbol represents an individual donor. Fig. S3: Representation of cell death and host response per donor. (**A**) Cell death (%), calculated from lactate dehydrogenase (LDH) release in PCLS, exposed to 10^6 PFU

of SARS-CoV-2 Early or Delta isolate, and IAV H1N1 or H5N1 48 h p.i. Each symbol represents an individual donor, whereas lines connect Mock and virus conditions of the same donor. (**B**, **C**, **D**, and **E**) IFN-β, IFN-λ1, IFN-λ2/3, IL-6, and IP10/CXCL10 mRNA expression levels per 18S rRNA 24 h p.i. Each symbol represents an individual donor, whereas lines connect Mock and virus conditions of the same donor for (**B**) SARS-CoV-2 Early isolate-, (**C**) Delta isolate-, (**D**) IAV H1N1-, and (**E**) H5N1-infected PCLS. Mock, black; SARS-CoV-2 early isolate, green; SARS-CoV-2 Delta isolate, blue; IAV H1N1, orange; IAV H5N1, yellow. Fig. S4: Correlation analysis of cell death and host response with tissue donor age. (**A**) Correlation of cell death and donor age for non-infected, SARS-CoV-2 Early isolate-, or Delta isolate-, and IAV H1N1-, or H5N1-infected PCLS. Association was tested using the Spearman rank correlation test. Each symbol represents an individual donor at 24 h (circle), 48 h (square), or 72 h p.i. (triangle). (**B**, **C**, **D**, and **E**) Correlation of IFN-β, IFN-λ1, IFN-λ2/3, IL-6, and IP10/CXCL10 mRNA expression levels per 18S rRNA and donor age. Each symbol represents an individual donor at 24 h, (circle) 48 h (square), or 72 h p.i. (triangle) of (**B**) SARS-CoV-2 Early isolate-, (**C**) Delta isolate-, (**D**) IAV H1N1-, and (**E**) H5N1-infected PCLS. Non-infected, black; SARS-CoV-2 early isolate, green; SARS-CoV-2 Delta isolate, blue; IAV H1N1, orange; IAV H5N1, yellow. Association was tested using the Spearman rank correlation test.

Acknowledgements
The authors would like to thank all study participants and their families. Furthermore, the authors acknowledge Lisa Butticaz, Noelle Donzé, and Teodora David for technical help.

Author contributions
MFC and MPA conceived and designed research; MB, CM, TZ, CC, DJ, BT, SE, BIOE, PD, TMM performed experiments; MB, CM, TZ, CC, BT, MFC, MPA analyzed data and interpreted results of experiments; MB, CM, TZ, CC, and BT prepared figures; MB, CM, MFC, MPA drafted manuscript; MB, CM, TZ, CC, DJ, PD, TMM, GZ, VT, MFC, MPA edited and revised manuscript; all authors approved final version of manuscript.

Funding
This work acknowledges support from the Lungenliga Bern, Switzerland to M.P.A. (Project ID "The impact of SARS-CoV-2 infection on the aged lung"), from the Bern Center for Precision Medicine (BCPM), Switzerland to M.F.C., and by intramural funding of the Institute of Virology and Immunology, Switzerland. The funders had no role in study design, data collection and analysis, decision to publish, or preparation of the manuscript.

Data availability
Data is provided within the manuscript or supplementary information files.

Declarations

Ethical approval and consent to participate
All human tissues were gathered and managed in accordance with the Declaration of Helsinki, and the study was approved by the Swiss Ethics Committee, Bern, Switzerland, approval number KEK-BE_2018-01801. Written informed consent was obtained from all donors before recruitment.

Consent for publication
Not applicable.

Competing interests
The authors declare no competing interests.

Author details
[1]Institute of Virology and Immunology, Bern, Switzerland. [2]Department of Infectious Diseases and Pathobiology, Vetsuisse Faculty, University of Bern, Bern, Switzerland. [3]Department for Pulmonary Medicine, Allergology and Clinical Immunology, Inselspital, Bern University Hospital, University of Bern, Bern, Switzerland. [4]Lung Precision Medicine (LPM), Department for BioMedical Research (DBMR), University of Bern, Bern, Switzerland. [5]Present Address: Graduate School for Cellular and Biomedical Sciences, University of Bern, Bern, Switzerland. [6]Department of General Thoracic Surgery, Inselspital, Bern University Hospital, University of Bern, Bern, Switzerland. [7]Department for Biomedical Research, University of Bern, Bern, Switzerland. [8]Multidisciplinary Center for Infectious Diseases (MCID), University of Bern, Bern, Switzerland. [9]European Virus Bioinformatics Center, Jena, Germany. [10]Present Address: Institute of Parasitology, Department of Infectious Diseases and Pathobiology, Vetsuisse Faculty, University of Bern, Bern, Switzerland. [11]Present Address: Institute of Virology, Freie Universitaet Berlin, Berlin, Germany. [12]Present Address: Spiez Laboratory, Federal Office for Civil Protection, Spiez, Switzerland.

Received: 23 October 2024 Accepted: 11 March 2025
Published online: 24 March 2025

References

1. Jain S, Self WH, Wunderink RG, Fakhran S, Balk R, Bramley AM, et al. Community-acquired pneumonia requiring hospitalization among U.S. Adults. N Engl J Med. 2015;373(5):415–27.
2. Kochanek KD, Murphy SL, Xu J, Arias E. Deaths: Final Data for 2017. Natl Viral Stat Rep. 2019. 68(9).
3. Musuuza JS, Watson L, Parmasad V, Putman-Buehler N, Christensen L, Safdar N. Prevalence and outcomes of co-infection and superinfection with SARS-CoV-2 and other pathogens: a systematic review and meta-analysis. PLoS ONE. 2021;16(5): e0251170.
4. Onder G, Rezza G, Brusaferro S. Case-fatality rate and characteristics of patients dying in relation to COVID-19 in Italy. JAMA. 2020;323(18):1775.
5. Jain S, Kamimoto L, Bramley AM, Schmitz AM, Benoit SR, Louie J, et al. Hospitalized patients with 2009 H1N1 influenza in the United States, April–June 2009. N Engl J Med. 2009;361(20):1935.
6. Bhat N, Wright JG, Broder KR, Murray EL, Greenberg ME, Glover MJ, et al. Influenza-associated deaths among children in the United States, 2003–2004. N Engl J Med. 2005. https://doi.org/10.1056/NEJMoa051721.
7. Zimmermann P, Nigel C. Coronavirus infections in children including COVID-19 an overview of the epidemiology, clinical features, diagnosis, treatment and prevention options in children. Ped Inf Dis J. 2020;39(5):355.
8. Adnot S, Bernard D, Lipskaia L, Trottein F. Cell senescence, a new target for respiratory viral infections: from influenza virus to SARS-CoV-2. Bull Acad Natl Med. 2023;207(2):193–8.
9. Schmitt CA, Tchkonia T, Niedernhofer LJ, Robbins PD, Kirkland JL, Lee S. COVID-19 and cellular senescence. Nat Rev Immunol. 2023;23(4):251–63.
10. Chen J, Kelley WJ, Goldstein DR. Role of aging and the immune response to respiratory viral infections: potential implications for COVID-19. J Immunol. 2020;205(2):313–20.
11. Martinez I, Garcia-Carpizo V, Guijarro T, Garcia-Gomez A, Navarro D, Aranda A, et al. Induction of DNA double-strand breaks and cellular senescence by human respiratory syncytial virus. Virulence. 2016;7(4):427–42.
12. Schulz L, Hornung F, Hader A, Radosa L, Brakhage AA, Loffler B, et al. Influenza virus-induced paracrine cellular senescence of the lung contributes to enhanced viral load. Aging Dis. 2023;14(4):1331–48.
13. Lee S, Yu Y, Trimpert J, Benthani F, Mairhofer M, Richter-Pechanska P, et al. Virus-induced senescence is a driver and therapeutic target in COVID-19. Nature. 2021;599(7884):283–9.
14. Weinheimer VK, Becher A, Tonnies M, Holland G, Knepper J, Bauer TT, et al. Influenza A viruses target type II pneumocytes in the human lung. J Infect Dis. 2012;206(11):1685–94.
15. Bui CHT, Chan RWY, Ng MMT, Cheung MC, Ng KC, Chan MPK, et al. Tropism of influenza B viruses in human respiratory tract explants and airway organoids. Eur Respir J. 2019. https://doi.org/10.1183/13993003.00008-2019.
16. Hui KPY, Chan LLY, Kuok DIT, Mok CKP, Yang Z-f, Li R-f, et al. Tropism and innate host responses of influenza A/H5N6 virus: an analysis of ex vivo and in vitro cultures of the human respiratory tract. Europ Resp J. 2017. https://doi.org/10.1183/13993003.01710-2016.
17. Hui KPY, Cheung MC, Perera R, Ng KC, Bui CHT, Ho JCW, et al. Tropism, replication competence, and innate immune responses of the coronavirus SARS-CoV-2 in human respiratory tract and conjunctiva:

an analysis in ex-vivo and in-vitro cultures. Lancet Respir Med. 2020;8(7):687–95.
18. Hönzke K, Obermayer B, Mache C, Fatykhova D, Kessler M, Dokel S, et al. Human lungs show limited permissiveness for SARS-CoV-2 due to scarce ACE2 levels but virus-induced expansion of inflammatory macrophages. Eur Respir J. 2022. https://doi.org/10.1183/13993003.02725-2021.
19. Wu W, Zhang W, Booth JL, Metcalf JP. Influenza A(H1N1)pdm09 virus suppresses RIG-I initiated innate antiviral responses in the human lung. PLoS ONE. 2012;7(11): e49856.
20. Hui KPY, Ho JCW, Cheung MC, Ng KC, Ching RHH, Lai KL, et al. SARS-CoV-2 Omicron variant replication in human bronchus and lung ex vivo. Nature. 2022;603(7902):715–20.
21. Pechous RD, Malaviarachchi PA, Banerjee SK, Byrum SD, Alkam DH, Ghaffarieh A, et al. An ex vivo human precision-cut lung slice platform provides insight into SARS-CoV-2 pathogenesis and antiviral drug efficacy. J Virol. 2024;6:114.
22. Usemann J, Alves MP, Ritz N, Latzin P, Muller L. Age-dependent response of the human nasal epithelium to rhinovirus infection. Eur Respir J. 2020. https://doi.org/10.1183/13993003.00877-2020.
23. Chason KD, Jaspers I, Parker J, Sellers S, Brighton LE, Hunsucker SA, et al. Age-associated changes in the respiratory epithelial response to influenza infection. J Gerontol A Biol Sci Med Sci. 2018;73(12):1643–50.
24. Liu G, Betts C, Cunoosamy DM, Aberg PM, Hornberg JJ, Sivars KB, et al. Use of precision cut lung slices as a translational model for the study of lung biology. Respir Res. 2019;20(1):162.
25. Alsafadi HN, Uhl FE, Pineda RH, Bailey KE, Rojas M, Wagner DE, et al. Applications and approaches for three-dimensional precision-cut lung slices disease modeling and drug discovery. Am J Respir Cell Mol Biol. 2020;62(6):681–91.
26. Rosales Gerpe MC, van Vloten JP, Santry LA, de Jong J, Mould RC, Pelin A, et al. Use of precision-cut lung slices as an ex vivo tool for evaluating viruses and viral vectors for gene and oncolytic therapy. Mol Ther Methods Clin Dev. 2018;10:245–56.
27. Akram KM, Yates LL, Mongey R, Rothery S, Gaboriau DCA, Sanderson J, et al. Live imaging of alveologenesis in precision-cut lung slices reveals dynamic epithelial cell behaviour. Nat Commun. 2019. https://doi.org/10.1038/s41467-019-09067-3.
28. Preuss EB, Schubert S, Werlein C, Stark H, Braubach P, Hofer A, et al. The challenge of long-term cultivation of human precision-cut lung slices. Am J Pathol. 2022;192(2):239–53.
29. Temann A, Golovina T, Neuhaus V, Thompson C, Chichester JA, Braun A, et al. Evaluation of inflammatory and immune responses in long-term cultured human precision-cut lung slices. Human Vaccines Therapeutics. 2017. https://doi.org/10.1080/21645515.2017.1264794.
30. Viana F, O'Kane CM, Schroeder GN. Precision-cut lung slices: a powerful ex vivo model to investigate respiratory infectious diseases. Mol Microbiol. 2022;117(3):578–88.
31. Siwczak F, Hiller C, Pfannkuche H, Schneider MR. Culture of vibrating microtome tissue slices as a 3D model in biomedical research. J Biol Eng. 2023;17(1):36.
32. Brügger M, Demoulins T, Barut GT, Zumkehr B, Oliveira Esteves BI, Mehinagic K, et al. Pulmonary mesenchymal stem cells are engaged in distinct steps of host response to respiratory syncytial virus infection. PLoS Pathog. 2021;17(7): e1009789.
33. Guler SA, Machahua C, Geiser TK, Kocher G, Marti TM, Tan B, et al. Dehydroepiandrosterone in fibrotic interstitial lung disease: a translational study. Respir Res. 2022;23(1):149.
34. Bel M, Ocana-Macchi M, Liniger M, McCullough KC, Matrosovich M, Summerfield A. Efficient sensing of avian influenza viruses by porcine plasmacytoid dendritic cells. Viruses. 2011;3(4):312–30.
35. Barut GT, Halwe NJ, Taddeo A, Kelly JN, Schon J, Ebert N, et al. The spike gene is a major determinant for the SARS-CoV-2 Omicron-BA.1 phenotype. Nat Commun. 2022;13(1):5929.
36. Lau SY, Wang P, Mok BW, Zhang AJ, Chu H, Lee AC, et al. Attenuated SARS-CoV-2 variants with deletions at the S1/S2 junction. Emerg Microbes Infect. 2020;9(1):837–42.
37. Livak KJ, Schmittgen TD. Analysis of relative gene expression data using real-time quantitative PCR and the 2−ΔΔCT method. Methods. 2001. https://doi.org/10.1006/meth.2001.1262.
38. Gielen V, Sykes A, Zhu J, Chan B, Macintyre J, Regamey N, et al. Increased nuclear suppressor of cytokine signaling 1 in asthmatic bronchial epithelium suppresses rhinovirus induction of innate interferons. J Allergy Clin Immunol. 2015;136(1):177–88.
39. Alves MP, Guzylack-Piriou L, Juillard V, Audonnet JC, Doel T, Dawson H, et al. Innate immune defenses induced by CpG do not promote vaccine-induced protection against foot-and-mouth disease virus in pigs. Clin Vaccine Immunol. 2009;16(8):1151–7.
40. Slater L, Bartlett NW, Haas JJ, Zhu J, Message SD, Walton RP, et al. Co-ordinated role of TLR3, RIG-I and MDA5 in the innate response to rhinovirus in bronchial epithelium. PLoS Pathog. 2010;6(11): e1001178.
41. Gielen V, Johnston SL, Edwards MR. Azithromycin induces anti-viral responses in bronchial epithelial cells. Eur Respir J. 2010;36(3):646–54.
42. Corman VM, Landt O, Kaiser M, Molenkamp R, Meijer A, Chu DK, et al. Detection of 2019 novel coronavirus (2019-nCoV) by real-time RT-PCR. Euro Surveill. 2020. https://doi.org/10.2807/1560-7917.ES.2020.25.3.2000045.
43. Hofmann MA, Renzullo S, Baumer A. Phylogenetic characterization of H5N1 highly pathogenic avian influenza viruses isolated in Switzerland in 2006. Virus Genes. 2008;37(3):407–13.
44. Goulter AB, Goddard MJ, Allen JC, Clark KL. ACE2 gene expression is up-regulated in the human failing heart. BMC Med. 2004. https://doi.org/10.1186/1741-7015-2-19.
45. Spackman E, Senne DA, Bulaga LL, Garber LP, Perdue ML, Lohman LTD, et al. Development of a real-time reverse transcriptase PCR assay for type A influenza virus and the avian H5 and H7 hemagglutinin subtypes. J Clin Microbiol. 2002. https://doi.org/10.1128/JCM.40.9.3256-3260.2002.
46. Contoli M, Message SD, Laza-Stanca V, Edwards MR, Wark PAB, Bartlett NW, et al. Role of deficient type III interferon-λ production in asthma exacerbations. Nat Med. 2006. https://doi.org/10.1038/nm1462.
47. Schafer MJ, White TA, Iijima K, Haak AJ, Ligresti G, Atkinson EJ, et al. Cellular senescence mediates fibrotic pulmonary disease. Nat Commun. 2017;8:14532.
48. Buckley ST, Ehrhardt C. The receptor for advanced glycation end products (RAGE) and the lung. J Biomed Biotechnol. 2010;2010:917108.
49. Skehel JJ, Waterfield MD. Studies on the primary structure of the influenza virus hemagglutinin. Proc Natl Acad Sci U S A. 1975. https://doi.org/10.1073/pnas.72.1.93.
50. Klenk HD, Rott R, Orlich M, Blödorn J. Activation of influenza A viruses by trypsin treatment. Virology. 1975. https://doi.org/10.1016/0042-6822(75)90284-6.
51. Lazarowitz SG, Choppin PW. Enhancement of the infectivity of influenza A and B viruses by proteolytic cleavage of the hemagglutinin polypeptide. Virology. 1975. https://doi.org/10.1016/0042-6822(75)90285-8.
52. Hoffmann M, Kleine-Weber H, Schroeder S, Kruger N, Herrler T, Erichsen S, et al. SARS-CoV-2 cell entry depends on ACE2 and TMPRSS2 and Is blocked by a clinically proven protease inhibitor. Cell. 2020;181(2):271–80.
53. Zhou P, Yang XL, Wang XG, Hu B, Zhang L, Zhang W, et al. A pneumonia outbreak associated with a new coronavirus of probable bat origin. Nature. 2020;579(7798):270–3.
54. Wrapp D, Wang N, Corbett KS, Goldsmith JA, Hsieh C, Abiona O, et al. Cryo-EM structure of the 2019-nCoV spike in the prefusion conformation. Science. 2020;3:237.
55. Liu Y, Liu J, Johnson BA, Xia H, Ku Z, Schindewolf C, et al. Delta spike P681R mutation enhances SARS-CoV-2 fitness over Alpha variant. Cell Rep. 2022;267:16396.
56. Turnquist C, Ryan BM, Horikawa I, Harris BT, Harris CC. Cytokine storms in cancer and COVID-19. Cancer Cell. 2020;38(5):598–601.
57. Rodrigues TS, de Sa KSG, Ishimoto AY, Becerra A, Oliveira S, Almeida L, et al. Inflammasomes are activated in response to SARS-CoV-2 infection and are associated with COVID-19 severity in patients. J Exp Med. 2021;218(3):20201707.
58. Killip MJ, Fodor E, Randall RE. Influenza virus activation of the interferon system. Virus Res. 2015;209:11–22.
59. Hayden FG, Fritz R, Lobo MC, Alvord W, Strober W, Straus SE. Local and systemic cytokine responses during experimental human influenza A

virus infection relation to symptom formation and host defense. J Clin Invest. 1998;101(3):643–9.
60. Peiris JS, Yu WC, Leung CW, Cheung CY, Ng WF, Nicholls JM, et al. Re-emergence of fatal human influenza A subtype H5N1 disease. Lancet. 2004;363(9409):617–9.
61. de Jong MD, Simmons CP, Thanh TT, Hien VM, Smith GJ, Chau TN, et al. Fatal outcome of human influenza A (H5N1) is associated with high viral load and hypercytokinemia. Nat Med. 2006;12(10):1203–7.
62. Sirinonthanawech N, Uiprasertkul M, Suptawiwat O, Auewarakul P. Viral load of the highly pathogenic avian influenza H5N1 virus in infected human tissues. J Med Virol. 2011;83(8):1418–23.
63. Hu B, Huang S, Yin L. The cytokine storm and COVID-19. J Med Virol. 2021. https://doi.org/10.1002/jmv.26232.
64. Hou YJ, Okuda K, Edwards CE, Martinez DR, Asakura T, Dinnon KH 3rd, et al. SARS-CoV-2 reverse genetics reveals a variable infection gradient in the respiratory tract. Cell. 2020;182(2):429–46.
65. Fahmi A, Brugger M, Demoulins T, Zumkehr B, Oliveira Esteves BI, Bracher L, et al. SARS-CoV-2 can infect and propagate in human placenta explants. Cell Rep Med. 2021;2(12): 100456.
66. Ziegler CGK, Allon SJ, Nyquist SK, Mbano IM, Miao VN, Tzouanas CN, et al. SARS-CoV-2 receptor ACE2 is an interferon-stimulated gene in human airway epithelial cells and is detected in specific cell subsets across tissues. Cell. 2020;181(5):1016–35.
67. Sungnak W, Huang N, Becavin C, Berg M, Queen R, Litvinukova M, et al. SARS-CoV-2 entry factors are highly expressed in nasal epithelial cells together with innate immune genes. Nat Med. 2020;26(5):681–7.
68. Van Slambrouck J, Khan M, Verbeken E, Choi S, Geudens V, Vanluyten C, et al. Visualising SARS-CoV-2 infection of the lung in deceased COVID-19 patients. EBioMedicine. 2023;92: 104608.
69. Bhatnagar J, Gary J, Reagan-Steiner S, Estetter LB, Tong S, Tao Y, et al. Evidence of severe acute respiratory syndrome coronavirus 2 replication and tropism in the lungs, airways, and vascular endothelium of patients with fatal coronavirus disease 2019: an autopsy case series. J Infect Dis. 2021;223(5):752–64.
70. Weis W, Brown JH, Cusack S, Paulson JC, Skehel JJ, Wiley DC. Structure of the influenza virus haemagglutinin complexed with its receptor, sialic acid. Nature. 1988. https://doi.org/10.1038/333426a0.
71. Shinya K, Ebina M, Yamada S, Ono M, Kasai N, Kawaoka Y. Influenza virus receptors in the human airway. Nature. 2006. https://doi.org/10.1038/440435a.
72. van Riel D, Munster VJ, de Wit E, Rimmelzwaan GF, Fouchier RAM, Osterhaus ADME, et al. H5N1 virus attachment to lower respiratory tract. Science. 2006. https://doi.org/10.1126/science.1125548.
73. Nicholls JM, Chan MCW, Chan WY, Wong HK, Cheung CY, Kwong DLW, et al. Tropism of avian influenza A (H5N1) in the upper and lower respiratory tract. Nat Med. 2007. https://doi.org/10.1038/nm1529.
74. Tumpey TM, Maines TR, Van Hoeven N, Glaser L, Solorzano A, Pappas C, et al. A two-amino acid change in the hemagglutinin of the 1918 influenza virus abolishes transmission. Science. 2007. https://doi.org/10.1126/science.1136212.
75. Yang Z-Y, Wei C-J, Kong W-P, Wu L, Xu L, Smith DF, et al. Immunization by avian H5 influenza hemagglutinin mutants with altered receptor binding specificity. Science. 2007. https://doi.org/10.1126/science.1135165.
76. Beigel JH, Farrar J, Han AM, Hayden FG, Hyer R, de Jong MD, et al. Avian influenza A (H5N1) infection in humans. N Engl J Med. 2005;353(13):1374.
77. WHO. Cumulative number of confirmed human cases for avian influenza A(H5N1) reported to WHO, 2003–2023 2023 [Available from: https://www.who.int/publications/m/item/cumulative-number-of-confirmed-human-cases-for-avian-influenza-a(h5n1)-reported-to-who-2003-2022-5-jan-2023.
78. Baggio S, L'Huillier AG, Yerly S, Bellon M, Wagner N, Rohr M, et al. Severe acute respiratory syndrome coronavirus 2 (SARS-CoV-2) viral load in the upper respiratory tract of children and adults with early acute coronavirus disease 2019 (COVID-19). Clin Infect Dis. 2021;73(1):148–50.
79. Madera S, Crawford E, Langelier C, Tran NK, Thornborrow E, Miller S, et al. Nasopharyngeal SARS-CoV-2 viral loads in young children do not differ significantly from those in older children and adults. Sci Rep. 2021;11(1):3044.
80. Bellon M, Baggio S, Jacquerioz Bausch F, Spechbach H, Salamun J, Genecand C, et al. Severe acute respiratory syndrome coronavirus 2 (SARS-CoV-2) viral load kinetics in symptomatic children, adolescents, and adults. Clin Infect Dis. 2021;73(6):e1384–6.
81. Jones TC, Biele G, Muhlemann B, Veith T, Schneider J, Beheim-Schwarzbach J, et al. Estimating infectiousness throughout SARS-CoV-2 infection course. Science. 2021. https://doi.org/10.1126/science.abi5273.
82. Bunyavanich S, Do A, Vicencio A. Nasal gene expression of angiotensin-converting enzyme 2 in children and adults. JAMA. 2020. https://doi.org/10.1001/jama.2020.8707.
83. Silva MG, Falcoff NL, Corradi GR, Di Camillo N, Seguel RF, Tabaj GC, et al. Effect of age on human ACE2 and ACE2-expressing alveolar type II cells levels. Pediatr Res. 2023;93(4):948–52.
84. Baker SA, Kwok S, Berry GJ, Montine TJ. Angiotensin-converting enzyme 2 (ACE2) expression increases with age in patients requiring mechanical ventilation. PLoS ONE. 2021;16(2): e0247060.
85. Camell CD, Yousefzadeh MJ, Zhu Y, Prata L, Huggins MA, Pierson M, et al. Senolytics reduce coronavirus-related mortality in old mice. Science. 2021. https://doi.org/10.1126/science.abe4832.
86. Seoane R, Vidal S, Bouzaher YH, El Motiam A, Rivas C. The interaction of viruses with the cellular senescence response. Biology (Basel). 2020. https://doi.org/10.3390/biology9120455.
87. Maggi F, Spezia ARPG, Focosi D, Lai LMM, Pistello M, Iure Ad, et al. Nicotine upregulates ACE2 expression and increases competence for SARS-CoV-2 in human pneumocytes. ERJ Open Res. 2021. https://doi.org/10.1183/23120541.00713-2020.
88. Leung JM, Yang CX, Tam A, Shaipanich T, Hackett T-L, Singhera GK, et al. ACE-2 expression in the small airway epithelia of smokers and COPD patients: implications for COVID-19. Eur Respir J. 2020;200(8):70.
89. Liu A, Zhang X, Li R, Zheng M, Yang S, Dai L, et al. Overexpression of the SARS-CoV-2 receptor ACE2 is induced by cigarette smoke in bronchial and alveolar epithelia. J Pathol. 2021. https://doi.org/10.1002/path.5555.
90. Wang S, Yao X, Ma S, Ping Y, Fan Y, Sun S, et al. A single-cell transcriptomic landscape of the lungs of patients with COVID-19. Nat Cell Biol. 2021;23(12):1314–28.
91. Kelley WJ, Zemans RL, Goldstein DR. Cellular senescence: friend or foe to respiratory viral infections? Eur Respir J. 2020. https://doi.org/10.1183/13993003.02708-2020.
92. Basisty N, Kale A, Jeon OH, Kuehnemann C, Payne T, Rao C, et al. A proteomic atlas of senescence-associated secretomes for aging biomarker development. PLoS Biol. 2020;18(1): e3000599.
93. Stegmayr J, Wagner DE. The dawn of the omics era in human precision-cut lung slices. Eur Respir J. 2021. https://doi.org/10.1183/13993003.00203-2021.
94. Chan MC, Cheung CY, Chui WH, Tsao SW, Nicholls JM, Chan YO, et al. Proinflammatory cytokine responses induced by influenza A (H5N1) viruses in primary human alveolar and bronchial epithelial cells. Respir Res. 2005;6(1):135.
95. Lee SM, Cheung CY, Nicholls JM, Hui KP, Leung CY, Uiprasertkul M, et al. Hyperinduction of cyclooxygenase-2-mediated proinflammatory cascade: a mechanism for the pathogenesis of avian influenza H5N1 infection. J Infect Dis. 2008;198(4):525–35.
96. Lee SM, Gardy JL, Cheung CY, Cheung TK, Hui KP, Ip NY, et al. Systems-level comparison of host-responses elicited by avian H5N1 and seasonal H1N1 influenza viruses in primary human macrophages. PLoS ONE. 2009;4(12): e8072.
97. Cheng X, Xu Q, Song E, Yang CF, Kemble G, Jin H. The hemagglutinin protein of influenza A/Vietnam/1203/2004 (H5N1) contributes to hyperinduction of proinflammatory cytokines in human epithelial cells. Virology. 2010;406(1):28–36.
98. Cheung C, Poon L, Lau A, Luk W, Lau Y, Shortridge K, et al. Induction of proinflammatory cytokines in human macrophages by influenza A (H5N1) viruses: a mechanism for the unusual severity of human disease? Lancet. 2002. https://doi.org/10.1016/S0140-6736(02)11772-7.
99. Maines TR, Szretter KJ, Perrone L, Belser JA, Bright RA, Zeng H, et al. Pathogenesis of emerging avian influenza viruses in mammals and the host innate immune response. Immunol Rev. 2008;225:68–84.

100. Carter MJ, Fish M, Jennings A, Doores KJ, Wellman P, Seow J, et al. Peripheral immunophenotypes in children with multisystem inflammatory syndrome associated with SARS-CoV-2 infection. Nat Med. 2020;26(11):1701–7.
101. Kalfaoglu B, Almeida-Santos J, Tye CA, Satou Y, Ono M. T-Cell hyperactivation and paralysis in severe COVID-19 infection revealed by single-cell analysis. Front Immunol. 2020;11: 589380.
102. McGonagle D, Ramanan AV, Bridgewood C. Immune cartography of macrophage activation syndrome in the COVID-19 era. Nat Rev Rheumatol. 2021;17(3):145–57.
103. Vanderbeke L, Van Mol P, Van Herck Y, De Smet F, Humblet-Baron S, Martinod K, et al. Monocyte-driven atypical cytokine storm and aberrant neutrophil activation as key mediators of COVID-19 disease severity. Nat Commun. 2021;12(1):4117.
104. Wang Q, Wu L, Yu J, Li G, Zhang P, Wang H, et al. Comparison of tumor and two types of paratumoral tissues highlighted epigenetic regulation of transcription during field cancerization in non-small cell lung cancer. BMC Med Genom. 2022. https://doi.org/10.1186/s12920-022-01192-1.
105. He D, Wang D, Lu P, Yang N, Xue Z, Zhu X, et al. Single-cell RNA sequencing reveals heterogeneous tumor and immune cell populations in early-stage lung adenocarcinomas harboring EGFR mutations. Oncogene. 2021. https://doi.org/10.1038/s41388-020-01528-0.
106. Aran D, Camarda R, Odegaard J, Paik H, Oskotsky B, Krings G, et al. Comprehensive analysis of normal adjacent to tumor transcriptomes. Nat Commun. 2017. https://doi.org/10.1038/s41467-017-01027-z.
107. Michalaki C, Dean C, Johansson C. The use of precision-cut lung slices forstudying innate immunity to viral infections. Curr Prot. 2022. https://doi.org/10.1002/cpz1.505.

Publisher's Note